# A PARAMETRIC RADIATIVE FORCING MODEL FOR CIRRUS AND CONTRAIL CIRRUS

**U. Schumann**[1], **B. Mayer**[1,2], **K. Graf**[1], **H. Mannstein**[1], **and R. Meerkötter**[1]

[1]*Deutsches Zentrum für Luft- und Raumfahrt, Institut für Physik der Atmosphäre, Oberpfaffenhofen, Germany*
[2]*Meteorologisches Institut, Ludwig-Maximilians-Universität, München, Germany*

## ABSTRACT

This paper presents a new, computationally efficient parameterization to compute the instantaneous radiative flux changes induced by thin cirrus (including contrail cirrus) at top of the atmosphere. The method is part of a new contrail cirrus prediction tool CoCiP. The model is being prepared to interpret cirrus cover and radiative irradiance values derived from Meteosat data. CoCiP computes the shortwave and longwave radiative forcing for given outgoing longwave radiation (OLR) and reflected solar radiation (RSR) irradiance values without contrails. This a priori information is taken from a numerical weather prediction model such as the forecast model of ECMWF. The parameterization contains several free model parameters which are determined by a least squares fit to an extensive set of forward calculations performed with the radiative transfer package libRadtran. The approximate results and the libRadtran results correlate better than 98%. Further improvements appear to be feasible.

Key words: cirrus; contrail; radiative forcing.

## 1. INTRODUCTION

Condensation trails (contrails) are aircraft induced cirrus clouds, which may contribute to global warming [22, 17]. This paper resulted from ongoing work in assessing the radiative forcing from aviation induced cirrus. In particular, this paper describes a new approach to calculate radiative forcing by contrail cirrus.

Based on METEOSAT 8 and 9 (Meteosat second generation, MSG) SEVIRI infrared (IR) data, the cirrus cover in the viewing area of Meteosat is derived using the MeCiDa algorithm developed at this institute [15]. In addition, the top-of-the-atmosphere irradiance of outgoing longwave radiation (OLR) is estimated from SEVIRI IR data. From the correlation between air traffic density and cirrus cover density, the contribution of aviation induced cirrus (AIC) is derived in part of the North Atlantic, overlapping with the North Atlantic traffic corridor [11]. By combining the AIC signal with the OLR-signal, an estimate of the aviation induced radiative LW-forcing is derived. The results indicate a rather large aviation-induced increase in cirrus cover and a corresponding radiative forcing.

In order to explain these results, and to extrapolate the results to the globe, a new tool for contrail cirrus prediction (CoCiP) has been developed [23]. The tool is used to simulate contrail cirrus resulting from a fleet of cruising aircraft, flight by flight, regionally or globally. The method predicts contrail cirrus for given air traffic and weather prediction data. It describes the life cycle of contrails using a Lagrangian Gaussian plume model with simple bulk contrail ice properties, without feedback to meteorology. The approximate model is designed to be computationally efficient for use in complex contrail cirrus simulations, with thousands of contrails. This paper describes the method used for fast approximate computation of the longwave (LW) and shortwave (SW) radiative forcing (RF) for an added contrail cirrus. Applications within CoCiP are to be described elsewhere.

## 2. METHOD

Instead of solving the radiation transfer problem locally, which would require considerable computational efforts, we introduce approximate model equations (Section 2.1) which allow to estimate the radiative forcing from input available from NWP model output and from the simulated contrail properties. Previous approximate methods to estimate the RF from cirrus [6] or from aerosol layers [3] refer to an additional layer in an otherwise cloud-free atmosphere, with dependencies on properties of the Earth surface (surface albedo and brightness temperature). Our approximation assumes that the radiative forcing (RF) by contrail cirrus represents a small perturbation to the outgoing irradiances in the longwave (LW) and shortwave (SW) spectral ranges at top of the atmosphere. These irradiances characterize the effective brightness temperature and the effective albedo of the possibly cloudy atmosphere without contrails. The RF is approximated mainly as a function of optical depth and temperature of the contrail, following previous suggestions [5, 3, 10, 19, 6] (see also Section 3). In addition certain model functions ac-

*Proc. 'Atmospheric Science Conference', Barcelona, Spain, 7–11 September 2009 (ESA SP-676, November 2009)*

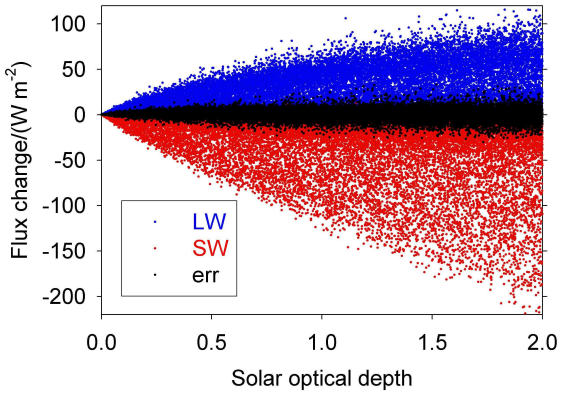


*Figure 1. Radiative forcing (RF) in the longwave and shortwave ranges versus solar optical depth $\tau$ (blue and red dots). The black dots represent the fit error for the net forcing (difference between $\mathrm{RF_{LW}} + \mathrm{RF_{SW}}$ results from the approximation and from libRadtran results)*

count for the dependence on solar zenith angle (SZA), particle radius, and particle habit. These dependencies are important since contrail cirrus does warm the Earth system during night, but may cool during day for large SZA, small particles, and particles with strong forward scattering [19]. The model contains several free model parameters which are determined from a fit to detailed radiative transfer calculations with the libRadtran package [18] (see Section 2.2). The fit method and the fit results are reported in 2.3.

### 2.1. Model equations of parameterized radiative forcing

The model computes the changes in net outgoing longwave and shortwave fluxes induced by an additional contrail cirrus (of 100 % cover) as a function of optical depth and temperature of the contrail cirrus, for given solar and terrestrial fluxes without contrails. The latter are available from the NWP or climate model results. The model computes the instantaneous RF at top of atmosphere (TOA), without stratospheric adjustment, for plane parallel clouds. For global RF calculations, the RF computed locally for contrail segments within CoCiP is added up weighted with the width and length of each contrail segment. In case of partially clouded atmospheres, we assume that the fluxes without contrail cirrus represent the partially clouded atmosphere below the contrail cirrus, and that the contrails overlap randomly with the rest of the clouds.

The model uses the following input to characterize the contrail cirrus, as available from the CoCiP model: $\theta$: solar zenith angle (SZA); $r$: effective contrail ice particle radius ($\mu$m); $T_C$: atmospheric temperature at the altitude of the contrail (K); $\tau$: contrail optical depth at 550 nm.

In addition, the model uses the following input from NWP data: $OLR$: outgoing longwave radiation at TOA (W/m$^2$); $RSR$: reflected solar radiation at TOA (W/m$^2$); $SDR$: solar direct radiation(W/m$^2$); $S_0$: the solar constant, with correction for the variable Sun-Earth-distance.

From these input values, the model computes the LW and SW RF per unit contrail area,

$$RF_{LW} = (OLR - \sigma_T\, T_C^{k_T})\,[1 - \exp(-\delta_\tau\,\tau)] \times F_{LW}(r) \geq 0, \quad (1)$$

with 6 fit parameters: $\sigma_T$, $k_T$, $\delta_\tau$ and 3 further parameters in $F_{LW}(r)$ (see below);

$$RF_{SW} = -\mu\, S_0\, (t_A - A_{\mathrm{eff}})^2\, C_{SW}(\mu,\tau) \times F_{SW}(r) \leq 0, \quad (2)$$

with effective albedo $A_{\mathrm{eff}} = RSR/SDR$, cosine of SZA $\mu = \cos\theta = SDR/S_0$, and 11 fit parameters (see below).

These approximations contain several functions (and therefore several fit parameters) to account for the dependencies on particle radius $r$ (in units of $\mu$m), optical depth $\tau$, and SZA in terms of $\mu$:

$$F_{LW}(r) = Q_{LW}(r)\frac{F_{LWr} + 100/(r + R_{LW})}{F_{LWr} + 100/(20 + R_{LW})} \quad (3)$$

$$Q_{LW}(r) = 1 - \exp(-Q_{LWr}\, r) \quad (4)$$

$F_{LW}(r)$ and $Q_{LW}(r)$ (and similar functions for SW, see below) are empirical formulas to consider the dependence on particle radius in the SW and LW spectral ranges at large and small particle radii, which determine the radiative forcing in addition to the most important variable $\tau$.

$$F_{SW}(r) = Q_{SW}(r)\frac{F_{SWr} + 100/(r + R_{SW})}{F_{SWr} + 100/(30 + R_{SW})} \quad (5)$$

$$Q_{SW}(r) = 1 - \exp(-Q_{SWr}\, r) \quad (6)$$

In addition, we use the effective optical depth

$$\tau_{\mathrm{eff}} = \tau/\mu, \quad (7)$$

reflectances

$$R_C(\tau_{\mathrm{eff}}) = \frac{\tau_{\mathrm{eff}}}{\Gamma_{SW} + \tau_{\mathrm{eff}}}, R'_C(\tau) = \frac{\Gamma'_{SW} + \tau/\gamma_{SW}}{1 + \tau/\gamma_{SW}}, \quad (8)$$

and SZA-depending factors

$$F_\mu(\mu) = \frac{(1-\mu)^{B_\mu}\,\mu^{C_\mu}}{(1/2)^{B_\mu + C_\mu}} - 1, \quad (9)$$

$$C_{SW}(\mu,\tau) = R_C(\tau_{\mathrm{eff}})(D_\mu + A_\mu\, R'_C(\tau)\, F_\mu(\mu)). \quad (10)$$

The radiative forcing in the LW, is constrained to positive values, so that contrails at low altitudes with high ambient

temperatures have zero contribution to $RF_{LW}$. Likewise, $RF_{SW}$ is constrained to negative values, though slightly positive values may occur for strongly absorbing atmospheres.

The form of the functions, e.g. in $F_{LW}(r)$, is constructed such that the fit parameters in these functions are linearly independent. For example they are selected to control mainly the shape of the functions but do not change the magnitude of the function values. That is the reason why the fit parameters occur both in the enumerator and the denominator of $F_{LW}(r)$.

### 2.2. Forward simulations with libRadtran

Forward simulations have been performed for a large set of horizontally homogeneous atmospheric and surface conditions with libRadtran [18]. libRadtran has been successfully validated in several model intercomparison campaigns and by direct comparison with observations. libRadtran offers a flexible interface to setup the atmospheric and surface conditions as well as a choice of different radiative transfer equation solvers. The approach is as described before [15, 12]. For the present application, the irradiances are computed using the DISORT 2.0 solver with 16 streams which allows accurate simulations of radiances. SW and LW irradiances are simulated using accurate correlated-k distributions [13, 10]. Ice cloud single scattering properties were parameterized, including the single scattering properties of hexagonal ice columns, for a wide range of effective radii. For scattering by ice crystals we use the double Henyey-Greenstein approximation, see Figure 9 in [14]. Profiles of pressure, temperature, water vapor, ozone concentration and other trace gases were taken from the TIGR-3 (Thermodynamic initial guess retrieval) data set [4].

The forward model is applied with and without an additional cirrus layer representing contrail cirrus. The difference between the net radiation fluxes with and without contrail cirrus determines the contrail cirrus cloud radiative forcing. In order to cover the variability of contrail RF with respect to contrail and ambient conditions, and a large set of fit parameters, the data set includes 27272 different atmospheres with different temperature and humidity profiles, over land and ocean, with and without upper troposphere ice clouds and lower level water clouds. Reflection of radiation at land and ocean surfaces is represented by non-isotropic wavelength-dependent bidirectional reflectance distribution functions (BRDF). The ocean BRDF is parameterized as a function of the 10 m surface wind speed [7, 20]. For the land surface BRDF we used the POLDER-1 BRDF database, Issue 2.00 [16]. The data are from CNES POLDER-1 onboard NASDA ADEOS-1. The data are grouped into the 17 IGBP (International Geosphere Biosphere Project) classes and into 12 NDVI (normalized difference vegetation index) classes for each IGBP class. These BRDFs were fitted using a three-parameter formula [21] for randomly selected pixels from eight different MODIS scenes (over Germany, Spain, Canada, and the Saharan desert, each for winter and summer). Each pixel has assigned a spectral albedo (determined by MODIS) as well as an IGBP class and an NDVI. The procedure covers a wide range of natural land surfaces. In order to cover the variability of contrail RF with respect to contrail and ambient properties, 22 of these properties are varied randomly in certain ranges. About 50 % of all cases include a layer of water clouds, and 50 % a layer of ice clouds; about 25 % are cloud free; and 25 % contain both water and ice clouds. The data set contains 6 different particle habits: spheres (with $5 - 25\,\mu$m radius), and randomly oriented solid columns, hollow-columns, rough-aggregates, rosettes, and plates [1, 2] (with $10 - 45\,\mu$m effective radius).

Further parameter variations include cosine of SZA: $0.2-1.0$; surface temperature: atmospheric temperature at z=0: $\pm 10K$; ice cloud optical thickness: $0-10$; ice cloud bottom: $6 - 10$ km; ice cloud height: $0.5 - 2$ km; water cloud optical thickness: $5 - 50$; water cloud effective radius: 5 - 15 $\mu$m; water cloud bottom: $1 - 2$ km; water cloud height: $0.5 - 6$ km; ocean surface wind speed (for ocean BRDF model): $1 - 15$ m/s.

Contrails have typically an optical depth of order $0.1 - 0.3$. Young contrails are composed of small near-spherical particles. From our CoCiP computations, we found that contrails contributing most to radiative forcing have particle radius of order $10 - 20\,\mu$m. Smaller particles have smaller cross-sections and larger particles sediment earlier. The near-spherical particle habits might best be approximated as droxtals [24] or spheres. Droxtals and spheres differ only slightly in the scattering phase functions and have similar single scattering properties; the largest differences occur in the extinction efficiencies at visible wavelengths, while differences at $11\,\mu$m are not as pronounced due to increased absorption within the ice particles [24]. Here we decided to use spherical particles, the optical properties of which can be accurately calculated by Mie theory. Larger contrail particles are non-spherical (as indicated by non-zero polarized Lidar returns [8]) and hence may be approximated as hexagonal solid columns or bullet rosettes. We suggest to assume 100 % droxtals for volume mean radius $0 - 5\,\mu$m, 70 % droxtals and 30 % solid columns for radii $5 - 10\,\mu$m, and 40 % droxtals und 30 % solid columns and 30 % 3D bullet rosettes for radii $10 - 30\,\mu$m. Larger contrail particles may have the same habit as suggested for natural cirrus [1].

Contrails are included in these forward simulations with variable depth and altitude values, ice water contents and particle habits. Presently, the libRadtran code allows for only 2 cloud types per altitude bin, which we use to treat water and ice clouds. Therefore, the computations are performed assuming the particle habit and size distribution of contrail ice particles to be the same as that of the surrounding cirrus layer (if present). We expect that this approximation is valid for given optical thickness, but further tests are planned. Contrail optical thickness is varied randomly in various cases: $0 - 2$, contrail bot-

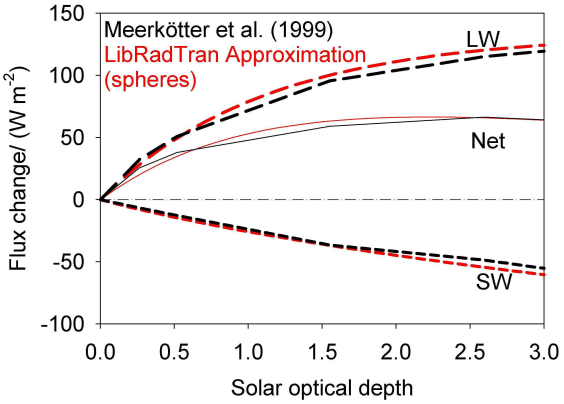


*Figure 2. Daily mean instantaneous short-wave (SW, short dashed), long-wave (LW, long dashed), and net forcing (full thin curve) versus* $0.55\,\mu$m *solar optical depth at top of the atmosphere for 100 % contrail cover for a mid-latitude continent reference case, at* $45°$ *latitude, with surface albedo of 0.2, surface temperature of* $20.8°$C*, and standard summer atmosphere. Cirrus layer between 10.8 and 11 km altitude, with effective contrail ice particle radius* $r = 16\,\mu$m*. Black curves, results of Meerkötter et al. [19] for spherical ice particles: Red curves: the same result for the present CoCiP model. It should be noted that these are daily mean values. The short wave mean value has been computed averaging over the day with one minute time step. For this application, the OLR and RSR values without contrail cirrus were derived from output of the previous study [19]:* $OLR = 279.63$ *W m*$^{-2}$*,* $RSR = 226.7, 204.2, 170.7, 126.5, 60.2,$ *and* $0$ *W m*$^{-2}$*, at SZA =* $19.1, 35.0, 50.7, 66.5, 82.2,$ *and* $90°$*, respectively.*

tom: $9 - 10$ km, contrail height: $0.5 - 1$ km. The atmospheric temperature at contrail cirrus mid-level varies between about $200 - 255$ K.

Figure 1 shows the computed RF versus optical depth. In these data the cooling in the SW dominates, mainly because of a large fraction of cases with large SZA, and non-spherical particle habits, which implies a cooling at least during morning or afternoon hours. We also see a weak nonlinear dependence of LW and SW RF magnitude on $\tau$.

### 2.3. Fit parameters

The model equations (see 2.1) contain 6 fit parameters for LW, and 11 fit parameters for SW, for each of the six habit classes, see Table 1. All fit parameters are restricted to positive values. The fit parameters have been computed by a least square fit where the sum $S = \Sigma_{all\ data} G(data - fit)^2$ assumes its minimum for variations in the free parameters. The set of parameters minimizing this sum is found numerically by univariate minimization. Table 1 lists the results obtained assuming equal relevance of all cases in the data set ($G = 1$). For $G = 1 + 1/(\tau + 0.1)$, thin contrail cirrus gets higher importance in the fits; as a result, the fit parameters change typically in the last digit of those listed in Table 1.

*Table 1. Best fit parameters for three of the six habits.*

| Parameter | spheres | solid columns | rosette -6 |
|---|---|---|---|
| $\sigma_T$ | 1.04E-5 | 0.89E-5 | 1.17E-5 |
| $k_T$ | 3.03 | 3.06 | 3.01 |
| $\delta_\tau$ | 0.89 | 0.82 | 0.74 |
| $F_{LWr}$ | 0.14 | 0.17 | 1. |
| $R_{LW}$ | 350. | 340. | 1.E6 |
| $Q_{LWr}$ | 0.30 | 0.24 | 0.21 |
| $t_A$ | 0.876 | 0.901 | 0.877 |
| $\Gamma_{SW}$ | 9.97 | 5.63 | 6.91 |
| $\Gamma'_{SW}$ | 17.2 | 17.8 | 13.3 |
| $\gamma_{SW}$ | 2.08 | 1.13 | 1.22 |
| $A_\mu$ | 0.0319 | 0.0350 | 0.0498 |
| $B_\mu$ | 1.47 | 1.42 | 1.39 |
| $C_\mu$ | 0.25 | 0.40 | 0.23 |
| $D_\mu$ | 0.89 | 1.02 | 1.01 |
| $F_{SWr}$ | 17.5 | 5.38 | 1.92 |
| $R_{SW}$ | 3.4 | 0.99 | 24. |
| $Q_{SWr}$ | 1.57 | 0.114 | 2.06 |

The results depend on the range of the selected properties in the libRadtran data base and the weighting of different input conditions. The forward simulation data set uses a random selection of the free input parameters. Otherwise, a deterministic relationship exists between fluxes and input parameters. The data set needs to be large enough to be representative for typical conditions regardless of the random realization. The robustness of the fit has been investigated by repeating the fit calculations with subsets of the data set, and further such studies are still to be performed.

It should be noted that the algorithm finds the best fitting parameters, but does not per se find the most suitable functional relationship. In fact, the version presented here is the result of a priori knowledge from the cited literature and some trial and error studies with various functions. Functions with too many parameters or with unsuitable forms (e.g. with linear dependencies between the fit parameters) showed up slow convergence when searching for the optimal fit. We expect that even better fits can be found by experimenting with other functions.

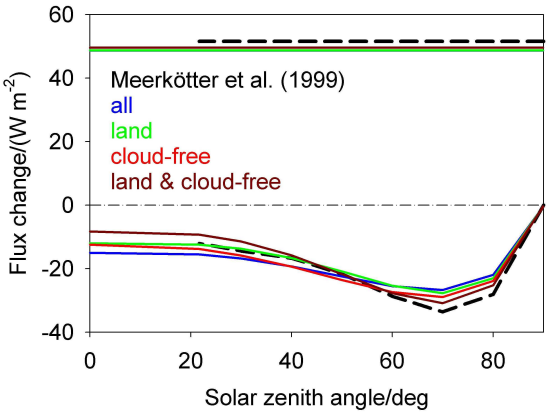


*Figure 3. Flux changes (top: LW, bottom: SW) versus solar zenith angle for $\tau = 0.52$, and other parameters as in Fig. 2. Dashed black curve: Meerkötter et al. [19]; full curves: present model; blue: all cases, green: land cases: brown: land and cloud-free (clear) cases.*

## 3. DISCUSSION

The dependence of the longwave forcing $RF_{LW}$ on the contrail temperature $T_C$ is similar to that used by Corti and Peter [6]; the exponent $k_T < 4$ accounts for the impact of upper tropospheric atmospheric water vapor on $RF_{LW}$. However, their model uses the surface temperature to compute the fluxes, which is appropriate only for cloud-free conditions. Instead, we use the OLR from the undisturbed, but possibly cloudy atmosphere (equivalent to a brightness temperature) from below the contrail cirrus. The factor $[1 - \exp(-\delta_\tau \tau)]$ measures the effective cloud emissivity; the fitted $\delta_\tau$ values range from 0.67 (for rough-aggregates) to 0.9 (for spheres), which includes the value 0.79 derived before [10] for solid columns.

The shortwave forcing $RF_{SW}$ tends to zero for $A_{\text{eff}} \rightarrow t_A$, which is of order unity. Because of molecular absorption in the atmosphere, the effective albedo never reaches unity even over ideally reflecting surfaces. (It has still to be investigated whether the parameterization can be further improved by accounting for gaseous and aerosol absorbers in the atmosphere below the contrail cirrus.) The quadratic dependence on $(t_A - A_{\text{eff}})$ is assumed as explained in [3, 19]. Tests with a variable exponent instead of the constant 2 showed that the value 2 is close to optimal. Tests with a term $t_A(1 - A_{\text{eff}})$ [6], instead of $(t_A - A_{\text{eff}})^2$ in Eq. (2) turned out to be less accurate.

Figure 1 shows the approximation error in relation to the SW and LW RF-values. The "exact" (from libRadtran) and "approximate" (from the new model) results correlate very well for longwave radiation flux changes: correlation coefficient $> 0.99$, root mean square (rms) error about 3 W m$^{-2}$. For the shortwave radiation flux the best fit has a correlation coefficient of $> 0.98$ and rms errors of 5 W m$^{-2}$. The relative errors (rms of difference between exact and approximate flux values relative to rms of exact flux values) are 2.7 % for LW, 4.3 % for SW and 7.5 % for net fluxes. (For comparison: 10 % for LW and 7 % for SW were reportd in [6]). The remaining scatter is due to the large variability of the atmospheres and surface properties and not explainable by one or a few of the free parameters (such as contrail altitude, presence of other clouds etc.). We found that the largest error contributions come from cloud-free atmospheres, presumably mainly because of the influence of the anisotropic BRDF.

Comparisons of results of this approximate model for spherical particles with previous "benchmark" results obtained with the matrix operator model [19] show excellent agreement for daily mean SW and LW radiative forcing, see Fig. 2. Even in the cloud-free case, the present approximation fits the earlier results [19] better than the approximation suggested in [6]. The results show large RF differences between contrails with different particle habits. While spheres tend to cause a net warming, the other habits are more likely causing a net cooling of the atmosphere during day-time because of far stronger (up to 100 %) SW RF.

The function $F_\mu(\mu)$ describes part of the SZA dependence of $RF_{SW}$. This dependence is stronger for thin cirrus than for thick ones [5], and this fact is accounted for by multiplying with the reflectance $R'_C(\tau)$, which is largest for small $\tau$. Figure 3 shows the SZA dependence, which is reasonably well represented, but shows still differences if fitted separately to the data for cases over land and ocean and for cloud-free and cloudy atmospheres. We expect that these differences are of minor importance for our application because of the large number of contrail cases; one could include separate parameterizations into CoCiP for land/ocean, clear/cloudy atmospheres in the future. We find somewhat larger differences relative to the benchmark results [19] in the SZA dependence for solid columns, mainly due to differences in the phase functions used. Whereas the libRadtran simulations were performed using the double Henyey-Greenstein approximation [14], The benchmark computations used a phase function computed assuming geometrical optics [19].

Figure 4 depicts the dependence on effective radius for constant $\tau$ and constant SZA. For spheres, $RF_{SW}$ and $RF_{LW}$ go to zero for particle radii $r$ small compared to the effective wavelength, presumably because of variations of single scattering albedo and asymmetry parameter. For large radii, the decline may be due to absorption. As expected, the radius dependences are stronger for SW than for LW radiation [2]. The SW RF for hexagons show a different behavior presumably because of missing cases with small radii for the non-spherical habits in the set of forward simulations.

## 4. CONCLUSIONS

A model has been presented which allows fast computations of the radiative forcing by cirrus, in particular by

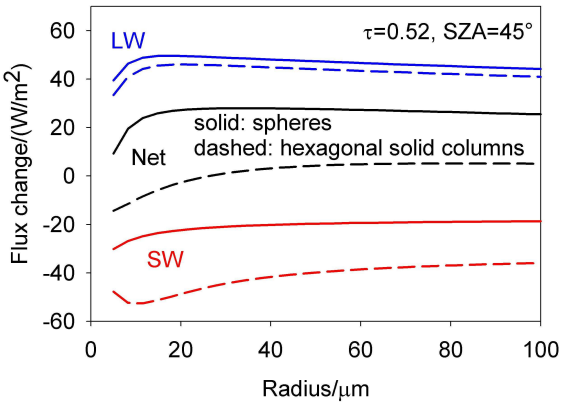


*Figure 4. RF versus effective radius for spheres and solid columns. $\tau = 0.52$, SZA = $45°$, and other parameters as in Fig. 2.*

contrail cirrus. The new idea of this approach is to compute the radiative forcing relative to a background state without contrail cirrus using the outgoing longwave and reflected shortwave output from NWP or climate model results. This makes the model applicable both for cloud-free and cloudy atmospheres. The relative errors are about 3 % for LW, 4 % for SW and 7.5 % for net fluxes. In view of other uncertainties, e.g. in the habits, this appears to be acceptable for our applications. The RF model is presently being applied within a contrail cirrus prediction tool CoCiP to predict the global radiative impact of contrail cirrus. Preliminary results suggest a far larger radiative impact from aviation induced clouds than estimated before for line-shaped contrails.

## ACKNOWLEDGMENTS

The POLDER-1 BRDF database Issue 2.00 has been produced by POSTEL from an original algorithm developed by Noveltis. The data are from CNES POLDER-1 onboard NASDA ADEOS-1. We thank Dr. Michael Ponater for valuable comments.

## REFERENCES

[1] Baum, B. A., Heymsfield, A. J., Yang, P., & Bedka, S. T. 2005a, J. Appl. Meteor., 44, 1885-1895

[2] Baum, B. A., Yang, P., Heymsfield, A. J., Platnick, S., King, M. D., Hu, Y.-X., & Bedka, S. T. 2005b, J. Appl. Meteor., 44, 1896-1911

[3] Charlson, R. J., Schwartz, S. E., Hales, J. M., Cess, R. D., Coakley, J. A., Hansen, J. E., & Hofmann, D. J. 1992, Science, 255, 423-430

[4] Chevallier, F., F. Cheruy, N.A. Scott, & A. Chedin 1998, J. Appl. Meteor., 37, 1385-1397

[5] Coakley, J. A., & Chylek, P. 1975, J. Atmos. Sci., 32, 409-418

[6] Corti, T., & Peter, T. 2009, Atmos. Chem. Phys., 9, 5751-5758

[7] Cox, C., & Munk, W. 1954, J. Marine Res., 13, 198-227

[8] Freudenthaler, V., Homburg, F., & Jäger, H. 1996, Geophys. Res. Lett., 23, 3715-3718

[9] Fu, Q. 1996, J. Clim., 9, 2058-2082

[10] Fu, Q., & Liou, K. N. 1992, J. Atmos. Sci., 49, 2139-2156

[11] Graf, K., Mannstein, H., Mayer, B., & Schumann, U. 2009, Aviation fingerprint in diurnal cycle of cirrus over the North Atlantic, Intern. Conf. Transport, Atmosphere and Climate-2 (Aachen and Maastricht), ed. R. Sausen et al. (in press)

[12] Gonzalez, A., Wendling, P., Mayer, B., Gayet, J.-F., & Rother, T. 2002, J. Geophys. Res., 107, 4693

[13] Kato, S., Ackerman, T. P., Mather, J. H., & Clothiaux, E. E. 1999, JQSRT, 62, 109-121

[14] Key, J. R., Yang, P., Baum, B. A., & Nasiri, S. L. 2002, J. Geophys. Res., 107, AAC 7 - 1 - 10

[15] Krebs, W., Mannstein, H., Bugliaro, L., & Mayer, B. 2007, Atmos. Chem. Phys., 7, 6145-6159

[16] Lacaze, R., Chen, J. M., Roujean, J. L., & Leblanc, S. G. 2002, Rem. Sens. Envir., 79, 84-95

[17] Lee, D. S., Pitari, G., Grewe, V., Gierens, K., Penner, J. E., Petzold, A., Prather, M. J., Schumann, U., Bais, A., Berntsen, T., Iachetti, D., Lim, L. L., & Sausen, R. 2009, Atmos. Env., doi:10.1016/j.atmosenv.2009.06.005

[18] Mayer, B., & Kylling, A. 2005, Atmos. Chem. Phys., 5, 1855-1877

[19] Meerkötter, R., Schumann, U., Minnis, P., Doelling, D. R., Nakajima, T., & Tsushima, Y. 1999, Ann. Geophysicae, 17, 1080-1094

[20] Nakajima, T., & Tanaka, M. 1983, JQSRT, 29, 521-537

[21] Rahman, H., Verstraete, M. M., & Pinty, B. 1993, J. Geophys. Res., 98, 20791-20801

[22] Schumann, U. 2005, Compt. Rend. Phys., 6, 549 - 565

[23] Schumann, U. 2009, A contrail cirrus prediction tool, Intern. Conf. Transport, Atmosphere and Climate-2 (Aachen and Maastricht), ed. R. Sausen et al. (in press)

[24] Yang, P., Baum, B. A., Heymsfield, A. J., Hu, Y. X., Huang, H.-L., Tsay, S.-C., & Ackerman, S. 2003, JQSRT, 79-80, 1159-1169